IJBBE International Journal of Biophotonics & Biomedical Engineering Vol. 3, No. 1, Winter-Spring, 2023

Review Article

Optical Coherence Tomography: A Brief Review

N. Moslehi Milani [a,b*]

a Department of Physics, Ahar Branch, Islamic Azad University, Ahar, Iran
b Biophotonics Research Center, Tabriz Branch, Islamic Azad University, Tabriz, Iran

***Corresponding Author Email: nmmilani@gmail.com**

DOI: 10.30495/ijbbe.2023.1993913.1032

ABSTRACT

Received: Sep. 8, 2023, Revised: Sep. 17, 2023, Accepted: Sep. 21, 2023, Available Online: Sep. 22, 2023

Optical coherence tomography (OCT) is a new imaging technique with a significant role in the field of medicine. It is a light-based non-invasive imaging method that provides high-quality cross-sectional and volumetric images. OCT technology was introduced in the early 1990s and advanced to produce quicker obtaining times and higher resolution. In this article, we discuss some of the recent advancements in OCT imaging systems. We will review a brief history and first operating principles including light coherence interferometry (LCI), time domain optical coherence tomography (TD-OCT) and Fourier domain optical coherence tomography (FD-OCT) contains two types: spectral domain optical coherence tomography (SD-OCT) and swept-source optical coherence tomography (SS-OCT). Also, we review recent emerging innovative OCT systems including Doppler OCT, polarization-sensitive optical coherence tomography (PS-OCT), high-resolution optical coherence tomography (HR-OCT), full-field optical coherence tomography (FF-OCT), wide-field optical coherence tomography (WF-OCT), optical coherence elastography (OCE), adaptive optics optical coherence tomography (AO-OCT), visible light optical coherence tomography (Vis-OCT), intraoperative optical coherence tomography (iOCT), hand-held optical coherence tomography (HH-OCT), and OCT in needle format.

KEYWORDS

cross-sectional imaging; low coherence interferometry; superluminescent light emitting diodes; ocular imaging; optical coherence microscopy.

I. INTRODUCTION

Optical Coherence Tomography (OCT) is a type of cross-sectional and volume imaging with high resolution of micro-internal structures in biological tissues, which is based on backscattered light echo measurement [1]. This imaging method was first developed in the field of ophthalmology and now it has been developed in other medical and even non-medical fields. This technique is called the non-invasive imaging method and so-called "optical biopsy". Light interference is based on the principle of Low Optical Coherence Interferometry (LCI) [2], which was first started in 1990 by Prof. Fercher's research group with deep and transverse scanning of the retinal pigment epithelium (RPE) of the human eye under in vivo conditions, and was reported in March 1991 [3,4]. Prof. Ippen and Prof. Fujimoto's research group, both at MIT, progressed the visualization of biological tissues from another perspective by using femtosecond light pulses [5] and by depicting the LCI signal to a color spectrum and viewing neighboring A-scans, they created a tomogram or cross-sectional picture, which was published

in November 1991 [1]. The first commercialized OCT system was introduced in 1996 with a scan rate of 100 scans per second [6], now commercial OCT devices have been developed to several million scans every second [7-10]. The first OCT system of the clinical ophthalmological world was the time domain OCT (TD-OCT) which had a low scanning speed of 400 A-scan/s, gradually after TD-OCT, spectral domain optical coherence tomography (SD-OCT) [11] and swept-source OCT (SS-OCT) [12-14] which are two different forms of Fourier domain OCTs (FD-OCTs), were introduced. These systems had scan rates of up to 100,000 A-scan/s. SD-OCT (spectrometer-based FD-OCT), was first introduced by Prof. Fercher et al in 1995 [15]. Swept-source optical coherence tomography (SS-OCT) was first demonstrated two years after SD-OCT in 1997 [16]. Hausler et al. presented the primary in vivo Fourier domain pictures of the skin in 1998 [17] and the initial in vivo human retinal tomograms by FD-OCT were published by Wojtkowski et al. in 2002 [18]. Now from 1990 to 2023 new OCT systems have been developed: wide-field OCT (WF-OCT), adaptive optics OCT (AO-OCT), polarization-sensitive OCT (PS-OCT), full-field OCT (FF-OCT), hand-held OCT (HH-OCT), intraoperative OCT (iOCT), Home-OCT, Ultra high-speed OCT, Ultra-high resolution OCT (UHR-OCT) and high-resolution OCT (HR-OCT), visible OCT (Vis-OCT), Photoacoustic/Optical coherence tomography (PA/OCT), vertical cavity surface emitting laser- Optical coherence tomography (VCSEL-OCT), and OCT in needle format. In this article, we will review the physical principles of OCT systems and introduce modern OCT systems along with their medical applications.

II. PHYSICAL PRINCIPLES OF OPTICAL COHERENCE TOMOGRAPHY

Optical coherence tomography (OCT) is usually compared to sonography, in both techniques waves are directed into the tissue under investigation and the back-scattered waves are considered and their retardation measured to extract deepness information. Optical coherence tomography generally utilizes the near-infrared (NIR) spectrum, which is much faster than ultrasound waves in sonography. The delay time of the reflected waves and the optical path difference in two separate paths are calculated in the interferometer (Fig. 1). The physical bases have been introduced in low coherence interferometry (LCI) [19,20]. OCT has features that are common to sonography and microscopes. The resolution of sonography imaging is usually 0.1-1 μm and relies on the sound wave frequency of 3-40 MHZ. Sound waves are transmitted at standard ultrasound frequencies with minimal absorption in biological tissue, and it is possible to image deep structures of the body. A resolution of 15-20 μm has been attained by frequencies of 100 MHZ, but these high frequencies are greatly degraded in biological tissues and the picturing depth is bounded to a few millimeters. Microscopes and confocal microscopes are imaging methods with much higher lateral resolution, i.e. 1 μm or better. Imaging is performed on the opposite plane and resolution is specified by optical diffraction. In biological tissues, deep imaging is possible until several hundred microns. Optical coherence tomography bridges the discrepancy between sonography and microscopy, with longitudinal (axial) resolution from 1 to 10 μm (10 to 100 times that of conventional sonography). In general, it can be said that the penetration depth of optical coherence tomography is greater than that of a microscope but less than that of an ultrasound, and the axial resolution of optical coherence tomography is less than that of a microscope but more than that of an ultrasound.

A. *Low coherence interferometry (LCI)*

In low coherence interferometry, the light beam coming from a light source is split into two different pathways (the path leading to the reference mirror and the path leading to the sample), The returning light from the two paths is combined at the output of the interferometer. The intensity of the interfering light is measured with an electrical signal by an optical detector (Fig. 1). This signal is a function of the optical path difference between the two paths

(or two interferometer arms). For a low-coherence light source such as a superluminescent light emitting diode (SLD) or a pulsed laser source, interference happens if the optical path difference of the two paths is comparable with the short coherence length of the source. An optical delay scan is obtained between the reference arm and the depth profile of the sample or A-scan, which is obtained by mechanically scanning a mirror setup in the reference arm. Extreme changes in refractive index at the interface between the layers in the specimen medium are shown as correspondent peaks in the interference patterning. Tissue can be expressed as the spatial distribution of refractive index on a microscopic scale [21-23]. The variation of refractive index distribution in the tissue causes strong light scattering.

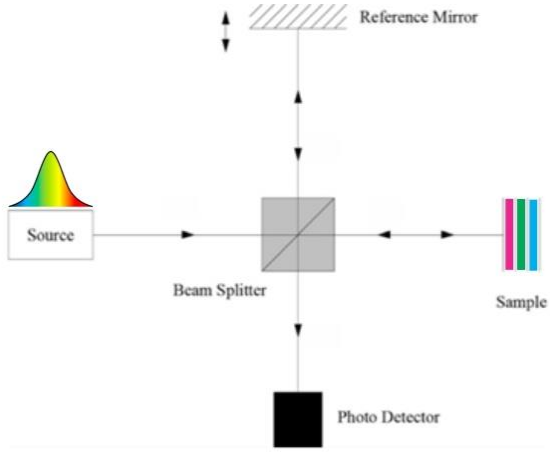

Fig. **1** Schematic illustration of a low coherence interferometry (LCI) setup.

B. *Operating principles of TD-OCT*

In TD-OCT, according to Fig. 2, the light beam of the source is divided into a reference beam and a sample beam, and the reflected beams from both pathways are recombined and stored by the detector. To record the figure of the depth of the specimen, the reference arm is A-scanned (the mirror mounted in the reference arm scans mechanically), and then transverse data is collected by storing A-scans at different neighboring positions of the sample.

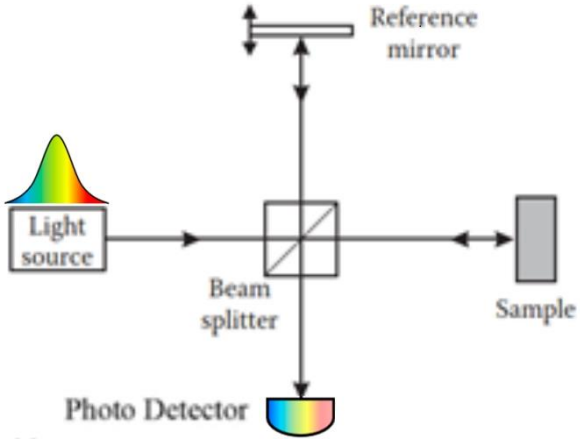

Fig. **2** Schematic setup of time domain optical coherence tomography (TD-OCT)

C. *Operating principles of SD-OCT*

In SD-OCT, the reference arm is fixed and the depth data is acquired by Fourier transform. No required mechanism for mechanical scanning, allows for faster scanning without losing image resolution (Fig. 3). SD-OCT is applied to retrieve the depth data from the spectral cross-checking method. The cross-spectral density (CSD) is measured in the detection arm of the interferometer using a spectrometer [11]. SD-OCT provides better detection sensitivity compared with the TD-OCT [24-26].

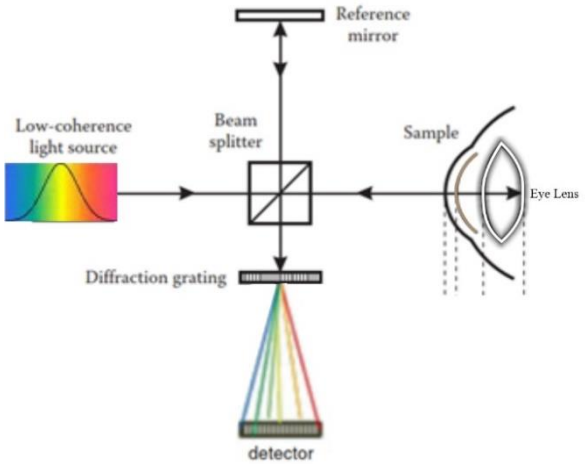

Fig. **3** Optical setup of spectral domain optical coherence tomography (SD-OCT)

D. *Operating principles of SS-OCT*

SS-OCT is a form of FD-OCT that uses a wide bandwidth fast scan pattern and has a light source that sweeps wavelengths in time and the reference mirror is fixed.

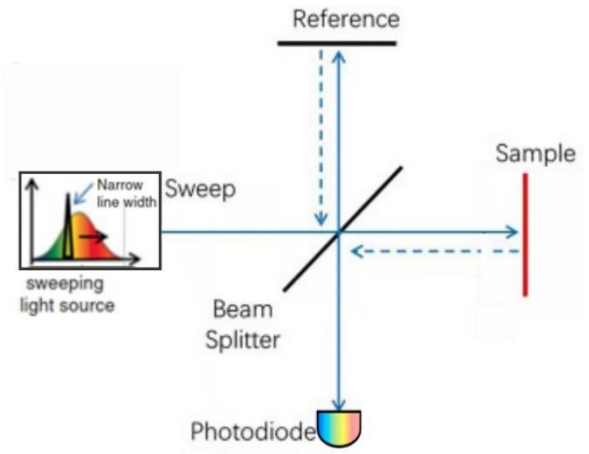

Fig. **4.** A typical setup for swept-source optical coherence tomography (SS-OCT)

The irradiated beam of the light source is divided into a reference arm and a sample arm, which collects the light sent back from inside the specimen, the interference pattern of the reference arm light beam and the sample arm light beam is observed by the light detector, while the monochrome frequency of the source is swept away. As well as this system is called optical frequency domain imaging (OFDI) [27]. There are three main differences between SD-OCT and SS-OCT [2]: 1- In SD-OCT, a wide-band light source illuminates the sample, but in SS-OCT, a single sweep laser rapidly sweeps various wavelengths to cover all of the broad spectrum. 2- Light reflection from the sample in SD-OCT is taken by a charged coupled device (CCD) camera, while in SS-OCT it is captured by a fast optical detector. 3- In most SS-OCT systems, a light source with a middle wavelength of approximately 1050 nm is used, while in SD-OCT, a central wavelength of 840 nm is used. The penetration depth of 1050 nm wavelength in tissue is greater than 840 nm.

E. *Physical concepts*

Lateral and axial resolution

Lateral resolution is described by the object and the focused medium ahead of the specimen. The lateral resolution is defined by the spot scale of the probe beam and for the Gaussian beam profile the spot scale is explained by the radius of the beam waist (w_0), where its intensity is reduced to $1/e^2$:

$$\delta x = \sqrt{2Ln2}\, w_0 \tag{1}$$

$$\delta x = \sqrt{2Ln2}\,\frac{\lambda_0}{\pi}\frac{2 f_{sys}}{nd} \tag{2}$$

$$\delta x = \sqrt{2Ln2}\,\frac{\lambda_0}{\pi}\frac{1}{NA} \tag{3}$$

where f_{sys}, n, d, λ_0, and NA are the focusing length of the system, the refractive index of the sample, the diameter of the beam (decline to $1/e^2$), wavelength in air, and numerical aperture respectively. Axial or longitudinal resolution for an OCT setup in air is equal to the coherence length of the source and proportional to the wavelength λ_0 and has an inverse relationship with bandwidth $\Delta\lambda$ which is the spectrum full width at half maximum (FWHM) [28]:

$$\delta z = l_c = \frac{2Ln2}{\pi}\frac{\lambda_0^2}{\Delta\lambda_{FWHM}} \tag{4}$$

Figure 5 shows the “Iso-resolution lines” for a given axial OCT resolution, required spectral bandwidth as a function of centric wavelength (there is a certain axial resolution at a certain central wavelength and a certain bandwidth). It is clear from the graphs that for longer wavelengths, the spectral bandwidth of the light must be increased to obtain the same axial resolution.

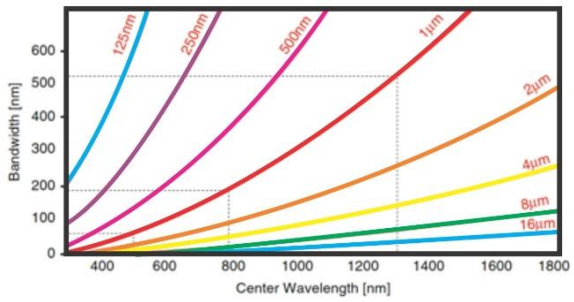

Fig. **5** OCT axial resolution (ranging from 16 to 0.125 µm) depends on both the optical bandwidth and the center wavelength. Dashed lines are for 500 nm, 800 nm, and 1300 nm, respectively [29]

Sensitivity

An important parameter of OCT imaging is detection sensitivity. Sensitivity is defined by the smallest detectable signal from the noise. A suitable definition of sensitivity is the ratio between the reflectivity of a perfectly reflective mirror ($R=1$) and the sample reflectivity $R_{S\min}$ which is a signal power equivalent to noise (or signal-to-noise ratio $SNR=1$) [20]:

$$S=\frac{1}{R_{S\min}} \tag{5}$$

or concerning dB is defined as follows:

$$S(dB)=10\log\frac{1}{R_{S\min}} \tag{6}$$

$R_{S\min}$ is the weakest reflectivity of the sample [28].

Field of view (FOV)

The scan angle defines the field of view (FOV) of a certain region on the sample, e.g. Retina. The twice maximum scan angle, $2\theta_{\max}$ explains the maximum field of view (Fig. 6). To screen a lateral field of view, an OCT beam scans the sample [30]. Describing the depth field of view (FOV) is unlike in TD-OCT and FD-OCT. In TD-OCT the area of depth FOV is restricted by the scanning domain of the reference light beam (and sensitivity of the system) whereas the depth field of view in FD-OCT is limited by the resolution of the spectroscopy device [28].

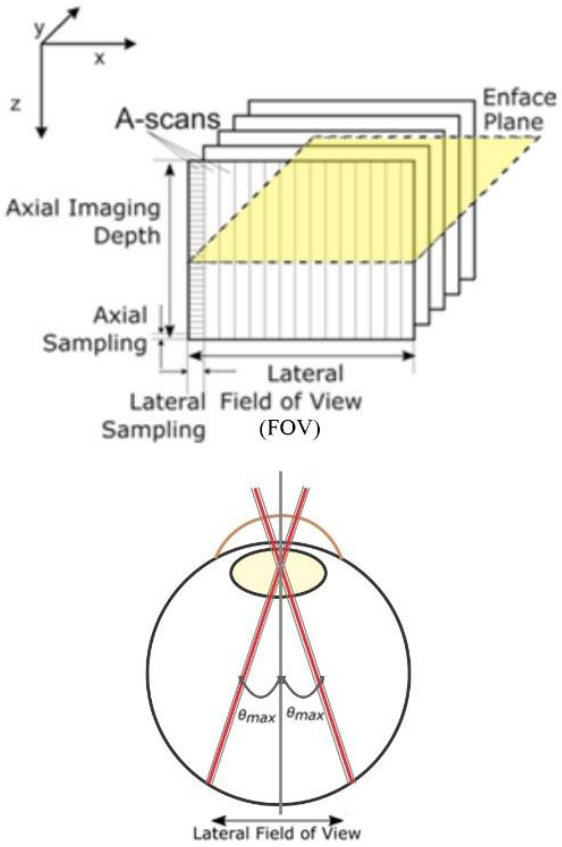

Fig. **6** Up: Axial and lateral sampling of OCT in three-dimensional volume. Down: Maximum lateral field of view (FOV) in retinal OCT.

III. OCT LIGHT SOURCES

Broadband light sources known as superluminescent light emitting diodes (SLDs) and wavelength-swept lasers are used as light sources for OCT systems. The major part of SLDs well-used for OCT is in the range of wavelength 800–900 nm and working in ocular SD-OCT set-ups. Wideband SLDs at 1300 nm are used in TD-OCT setups for industrial utilization [23].

A. *Superluminescent light-emitting diodes (SLDs)*

Superluminescent light-emitting diodes (SLDs) are the most important light sources for TD-OCT and SD-OCT imaging. SLDs are optoelectronic devices with the properties of

both a laser diode (LD) and light light-emitting diode (LED) [31]. These diodes work in the amplified spontaneous emission (ASE) regime [32]. The first SLD was presented in 1971 by Kurbatov et al. [33]. The first generation of SLDs was used in fiber-optic gyroscopes [34,35]. The second generation of SLDs was developed after a victorious illustration of OCT capability and its potential compared with other imaging techniques in medicine [35]. OCT systems needed more capable SLDs than those in the earlier 1990s, especially with an output power of a minimum of 10 mW. Thorlabs company has introduced many SLD devices designed for OCT applications with center wavelengths from 770 nm to 1610 nm [39]. Information on the spectrum and various operating parameters is available on Thorlabs' online website [39].

Principles of SLD operation

SLDs merge the directive beam of the laser diodes with the broadband emission spectrum of the light-emitting diodes [36]. An ideal SLD has two facets with zero reflectivity in an active channel (Fabry-Perot cavity in epitaxial active layer). In a real SLD, the end facets are designed with low reflectivity, for suppression of laser feedback. In the active layer of an SLD, two counter-propagating beams of ASE are moving throughout the length of the active cavity. For the approximation of output power, SLD is characterized by an easy model that takes into account the uniform distribution of the carrier's density along the cavity region of SLD. This model was investigated in some research papers [37,38]. The broadband spectrum and short coherence length of the SLD improve the axial resolution of OCT images. A typical SLD structure and its package that is used for the OCT system has been shown in Fig 7.

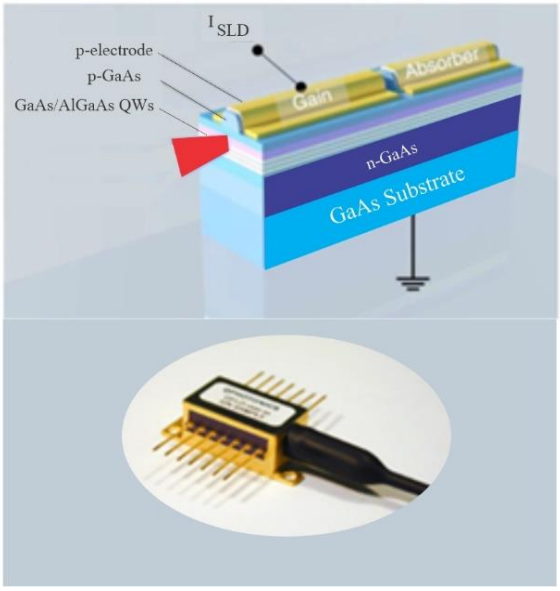

Fig. **7** Structure of a typical superluminescent light emitting diode (SLD) and a kind of SLD package for OCT system

B. *swept source laser technology for OCT*

Wavelength-swept lasers are used in OCT systems widely [40-42], especially in late years, swept laser high technology has been impressive in advancing OCT application in biomedical imaging. In general, swept sources for optical coherence tomography are tunable lasers with an uncommon set of operating parameters [43]. They require different components, different cavity designs, and innovative operating regimes. Many other performance standards exist for swept lasers. As yet since 2003 many swept lasers have been demonstrated with wavelength range of 1050-1558 nm and sweep speed range of 0.25-11500 kHz. Various laser types and their operational parameters were collected in [43]. Additional information is available in [35] and [43-45].

IV. INNOVATIVE OCT SYSTEMS

A. *Doppler optical coherence tomography or Optical Doppler tomography (ODT)*

Optical coherence tomography technique, in addition to examining the tissue structure, can

estimate the functional characteristics of the specimen, such as blood flow, applying Doppler OCT angiography. The frequency of the light beam changes when it is scattered by mobile red blood cells, and total frequency change is related to the blood flow velocity according to [46,47]:

$$\Delta f = \frac{1}{2\pi}\left(\vec{k}_s - \vec{k}_i\right)\cdot\vec{V} \quad (7)$$

Where $\vec{k}_s$ and $\vec{k}_i$ are wave vectors of scattered and incident light respectively, and $\vec{V}$ is the velocity vector of the moving blood cell (Fig. 8). Assuming the angle between the velocity of the blood cell and incident beam is θ, the Doppler shift equation is simplified to [46]:

$$\Delta f = \frac{2nV\cos\theta}{\lambda_0} \quad (8)$$

Where λ_0 and n are the vacuum middle wavelength of the light source and refractive index of the medium. The obtained information by optical Doppler tomography (ODT) provides a contrast-free method to visualize and determine the amount of retina blood in vivo. These results help to diagnose pathological diseases for example diabetic retinopathy and glaucoma. The OCT scattered signal from the blood vessels (mostly with red blood cells) displays much more changes compared with the OCT signal originating from the scanned stationary tissue [4]. Doppler optical coherence tomography merges the principle of Doppler with OCT to achieve high-resolution images of tissue morphology and blood flow together. Doppler OCT only measures the component of velocity parallel to the OCT probe beam, two OCT light beams with constant offset in the incident angles can be used to measure the pure velocity and volume flow velocity [48,49]. This measuring demands particular hardware that is not consistent with conventional single-beam OCTs. Srinivasan et al. developed OCT Doppler to calculate cerebral blood flow [50] and Bauman et al. calculated total retinal blood flow (TRBF) by ultrafast SS-OCT [46]. Doppler OCT has many utilizations in biomedical research and clinical medicine caused by its extremely high resolution and spatial sensitivity. Various applications of Doppler optical coherence tomography are as follows: screening for vasoactive medical drugs, observing tissue structure changes and hemodynamics after drug involvement and dynamic therapy, assessing the depth of burn injuries, and cortical hemodynamic mapping for brain research.

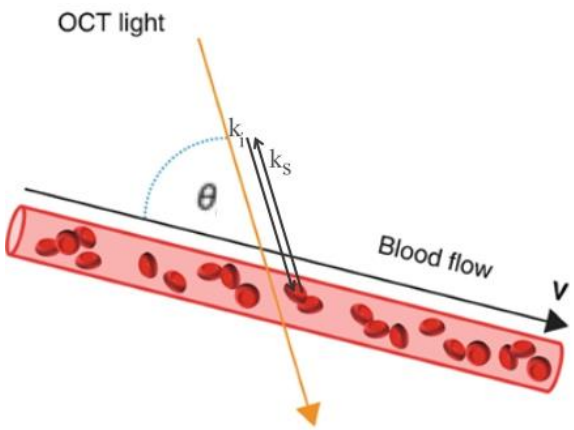

Fig. **8** Symbolic figure of blood flow (red blood cells) and light beam angle in Doppler optical coherence tomography

While Doppler OCT is capable of estimating blood flow in large blood vessels [51,52], it is difficult to detect the steady flow in small-scale blood vessels due to the bulk movement of the tissue. In the picturing of retinal blood vessels, Doppler optical coherence tomography confronts an extra limitation that most of the vessels are almost vertical to the OCT beam, and the ability to detect the Doppler shift signal is highly dependent on the incident angle of the beam. Up to now, various research groups have measured the total retinal blood flow by Doppler optical coherence tomography [51,53,54].

B. *Polarization-sensitive OCT (PS-OCT)*

Polarization-sensitive optical coherence tomography was first introduced in 1992 [55] and it is dependent on the form of polarized light that alters through several light-tissue interactions [2]. The features used in PS-OCT are birefringence, dichroism, and optical axis orientation, but mainly PS-OCT works by evaluating the backscattered polarization state and estimating birefringence in the sample tissue [55]. In a specimen, the double refractive index is based on the direction of polarization of the light beam, so the polarized component forwards the slow axis and undergoes a phase delay compared to the polarized component alongside the fast axis. If the variation of refractive index, Δn, is known, the measurement of retardation of δ, makes the possibility of determining the thickness of the birefringent sheet in the retina [30]. It is possible to distinguish eye structures based on the characteristics that change the state of polarization, for example, birefringence in the sclera, polarization preservation in photoreceptors, and depolarization in RPE are used. PS-OCT has also been employed in many utilizations, including correlation of burn depth with reduce of birefractivity [56], measurement of retinal nerve layer birefringence [57,58], and view of the start and going forward of caries lesions [59]. PS-OCT was first introduced in TD-OCT technology, but now it is used as SS-OCT and SD-OCT [60,61] for imaging several visual structures like the macula and peripheral retina [62-64].

C. *High-resolution OCT (HR-OCT) and ultra-high-resolution OCT (UHR-OCT)*

The performance of optical coherence tomography is principally found by longitudinal (axial) resolution, lateral resolution, sensitivity, and information achievement characteristics containing speed [65]. Optical coherence tomography can attain high-depth resolutions separate from numerical aperture (NA). According to Eq. (4) axial or depth resolution is reversed relative to the bandwidth of the light spectrum and squarely proportional to the middle wavelength of the light source (λ_0^2). To improve the longitudinal resolution of OCT, either the spectral bandwidth should be increased or the central wavelength should be reduced, and this is the basis of high and ultrahigh-resolution OCT [55]. Refining the axial resolution in optical coherence tomography is challenging and requires the utility of very complex optical sources with wide bandwidth. Figure 5 shows the Iso-Resolution lines and it is possible to find the necessary bandwidth for an assumed central wavelength to obtain the desired OCT axial resolution. A typical HR-OCT has a longitudinal resolution of 3 μm, which can obtain clearer images of choriocapillaris vasculature [55,66].

D. *Full-field optical coherence tomography (FF-OCT) or full-field optical coherence microscopy (FF-OCM)*

In TD-OCT and FD-OCT, image information is taken along pillar-shaped sections of the specimens and then the image is obtained by scanning the beam across the specimen surface [67]. Variously, full-field optical coherence tomography (FF-OCT) [68-71], provides enface images (a surface slab parallel to the sample area) without beam scanning. FF-OCT distinguishes the interferometric signal in the surface of the specimen at a specified depth and thus directly obtains a two-dimensional slice image [72]. Currently, FF-OCT captures two-dimensional enface images of visual tissue at various depths, and these images can be used to reassemble three-dimensional volumetric images until 1 μm resolution. Recently, human retinal ganglion axons have been reviewed by FF-OCT [73].

E. *Wide-field OCT (WF-OCT) and ultra-widefield OCT (UWF-OCT)*

Conventional OCT imaging system is often limited to $20^\circ \times 20^\circ$ the narrow field of view (narrow FOV) [74]. Higher degrees of FOV were introduced by wide field and ultra-wide field OCT systems (WF-OCT with the field of

view $40^{\circ}-45^{\circ}$ and UWF-OCT with FOV until 200°). The first UWF-OCT was suggested by Klein et al. [75] and was based on an ultrafast SS-OCT with a mode-locked 1050 nm laser. The utilization of frequency domain mode-locked lasers as an OCT light source was first presented by Wojtkowski, Huber, and Fujimoto in 2006 [76].

F. *Optical coherence elastography (OCE)*

An imaging technique called elastography produces elastogram images depending on the mechanical characteristics of a tissue [77]. The use of optical coherence tomography (OCT) in elastography known as optical coherence elastography (OCE) was first presented by Schmitt in 1998 [78]. This method is an alternative to manual (touch) exploration by physicians in a suspicious area. Touch is limited due to subjectiveness, low structural resolution, and low sensitivity. Originally, elastography was progressed using ultrasound [79] and magnetic resonance imaging (MRI) [80] as basic visualization methods. There are three basic steps in elastography: 1. A mechanical weight enters on specimen. 2. Displacement of the specimen is determined in reaction to the weight. 3. A specimen's mechanical characteristic is approximated from the calculated displacement. Prostate and Breast cancers are among the cases tested by elastography. Many eye diseases are associated with changes in the mechanical characteristics of the tissue: keratoconus, presbyopia (hardening of the lenses), glaucoma (accompanied by hardening of the sclera), and arteriosclerosis (decreasing the elasticity of blood vessels) [30]. Applications of OCE are currently in their infancy.

G. *Adaptive optics OCT (AO-OCT)*

Adaptive optics aims to compensate for optical aberrations using an adaptive optical element, for example, a deformable mirror. Adaptive optics was originally advanced to decrease dynamic wavefront errors in astronomical visualization [81]. In ophthalmology, AO-OCT is used to improve and remove monochromic aberrations from transmitted light through visual tissues for example cornea and lens. Adaptive optics systems estimate monochromic aberrations that occur in the eye and correct them by applying wavefront sensors and deformable mirrors.

H. *Visible light OCT (Vis-OCT)*

So far, all existing OCT systems applied in ophthalmology work in the range between wavelength 0.8 µm and 1.3 µm (near-infrared range). Vis-OCT was first introduced and described by Povazay et al. [82]. The utilization of visible wavelengths in the OCT light source is associated with restrictions and challenges: The optical device must be precisely corrected for chromatic deviations, and worthwhile wideband optical sources are not economically accessible. Additionally, due to the photochemical performance potential of blue light and the limitations of laser illumination which lead to reduced sensitivity of the OCT apparatus, it is a fundamental problem. The most critical restriction of Vis-OCT is the lack of access to intact structures under the retinal pigment epithelium (RPE) cause of the high absorption of visible light. Hence, the vascular system of the retina (capillaries and vessels) and choroid cannot be observed and evaluated with Vis-OCT compared to OCTA. Vis-OCT, despite the disadvantages, has major advantages [30]: 1. Both lateral resolution and specifically the longitudinal resolution of retinal OCT pictures can be remarkably improved. According to Eq. (4) it is clear that the utilization of a wide visible range at shorter wavelengths (450-700 nm) extends the longitudinal resolution to the sub-micron range, which is 8 times larger than the common infrared OCT by central wavelength 880 nm with a bandwidth of 80 nm. 2. Backscattered spectral information can be applied for spectroscopic determination. By absorption graphs for oxygenated and deoxygenated hemoglobin the information obtained in Vis-OCT can be applied to calculate the oxygen saturation of arterial blood and venous blood [83]. Oxygen saturation is described as the percent of oxygen-saturated hemoglobin (HbO_2) as to the entire quantity of oxygenated and deoxygenated hemoglobin [30]:

$$= \frac{\text{oxygen saturation (\%)}}{\text{oxygenated hemoglobin}} = \frac{\text{oxygenated hemoglobin}}{\text{oxygenated hemoglobin} + \text{deoxigenated hemoglobin}} \quad (9)$$

I. *Intraoperative optical coherence tomography (iOCT)*

Intraoperative optical coherence tomography (iOCT) is a recently developed OCT application for real-time intraoperative diagnostic visualizing. Intraoperative OCT supplies depth conception for surgeons besides ordinary surgical procedures. It also allows surgeons to view OCT imaging directly in the operating room in real time. The digital system integrated with iOCT allows surgeons to check the OCT data without leaving the operating room. iOCT may facilitate the delivery of therapeutic drugs, for example, tissue plasminogen activator [84] or electrode array placement for subretinal implants [55,85]. In ophthalmology clinics, iOCT provides fast non-contact micrometric scale visualization to observe the morphology of the retina and the anterior part of the eye (cornea). iOCT is also used in non-ophthalmic microsurgery, microsurgeries are used to handle and rebuild micron or millimeter-scale structures for example small vessels, nerves, and membranes. Conventional surgical microscopes provide just a little understanding of the 3rd dimension, and depth details must be deduced by the surgeon. iOCT can allow a direct understanding of the depth dimension, which can significantly ease surgical procedures in addition to pre-operation and post-operation assessment. In addition, it has been used to image human cartilage in usual knee joints and arthritis knees throughout open knee surgery. Blood vessels and nerves that are not easily seen under an ordinary microscope have been identified in iOCT images [86]. Tumors of the brain have been analyzed by high-resolution OCT, and the ability of iOCT for intraoperative usage has been demonstrated [87].

J. *Hand-held OCT*

Hand-held OCTs have been designed to solve the non-portability problem of commercial OCTs used in clinics [55,88], these OCTs are helpful for the young population as well as infants [89-91]. Manual OCT usually consists of two parts: 1- Light handset part 2- The base part which includes the light source, spectroscope, and data processor with the corresponding screen. The first hand-held OCT systems were developed for cases like babies who are not able to stand in front of optical scanning at OCT [92]. Hand-held OCT imaging is used during surgery to detect small bleeding caused by instrument manipulation. This information helps the surgeon estimate the amount of exfoliation needed.

K. *OCT in needle format*

OCT imaging is limited in clinical utilizations due to its very limited imaging depth (2-3 mm) in tissue [35]. OCT needle probes [93] can be designed using minimized fiber optic probes, which suggests its ability for deep body imaging. Several applications are expanding, including cancer diagnosis [94,95], lung imaging [96,97], eye imaging [98,99], and brain imaging [100,101]. OCT's high-speed hand-held needle scanners allow clinicians to perform in vivo imaging in real-time.

V. CONCLUSION

In this article, we reviewed the newest medical imaging method, optical coherence tomography, from its emergence to the latest developments. Our review includes a brief history and principles of the physical concepts of time domain, spectral domain, and swept-source optical coherence tomography systems, together with a review of their modern types for medical applications, especially in ophthalmology. The development and improvement of applied technologies in the domain of optical coherence tomography is a very active zone in the research area. This

article is a small step in the direction of expanding the view on this subject.

ACKNOWLEDGMENT

The author appreciates for helpful support of Prof. H. Tajalli, chancellor of the Biophotonics Research Center in Islamic Azad University of Tabriz (IAUT).

REFERENCES

[1] D. Huang, E.A. Swanson, C.P. Lin, J.S. Schuman, W.G. Stinson, W. Chang, M.R. Hee, T. Flotte, K. Gregory, C.A. Puliafito, and J.G. Fujimoto, "Optical coherence tomography," Science, vol. 254, pp. 1178–1181, 1991.

[2] T. Kostanyan, G. Wollstein, and J. S. Schuman, "New developments in optical coherence tomography," Current opinion in ophthalmology, vol.26, pp. 110, 2015.

[3] A. F. Fercher and E. Roth, "Ophthalmic laser interferometry," In Optical instrumentation for biomedical laser applications, vol. 658, pp. 48-51. 1986.

[4] C. K. Hitzenberger, "Optical measurement of the axial eye length by laser Doppler interferometry," Investigative ophthalmology & visual science, vol. 32, pp. 616-624, 1991.

[5] J. G. Fujimoto, S. de Silvestri, E. P. Ippen, C. A. Puliafito, R. Margolis, and A. Oseroff, "Femtosecond optical ranging in biological systems," Optics letters, vol.11, pp. 150-152, 1986.

[6] M. Everett, S. Magazzeni, T. Schmoll, and M. Kempe, "Optical coherence tomography: From technology to applications in ophthalmology," Translational Biophotonics, vol.3, pp. e202000012, 2021.

[7] W. Wieser, B. R. Biedermann, T. Klein, C. M. Eigenwillig, and R. Huber, "Multi-megahertz OCT: High-quality 3D imaging at 20 million A-scans and 4.5 GVoxels per second," Optics express, vol. 18, pp. 14685-14704, 2010.

[8] W. Wieser, B. R. Biedermann, T. Klein, C. M. Eigenwillig, and R. Huber, , "High-quality 3-D imaging with multimegahertz OCT," Optics and Photonics News, vol. 21, pp. 28-28, 2010.

[9] T. S. Kim, J. Joo, I. Shin, P. Shin, W. J. Kang, B. J. Vakoc, and W. Y. Oh, "9.4 MHz A-line rate optical coherence tomography at 1300 nm using a wavelength-swept laser based on stretched-pulse active mode-locking," Scientific Reports, vol. 10, pp. 9328 (1-9), 2020.

[10] S. Grelet, P. B. Montague, and A. Podoleanu, "Towards sub-5 µm axial resolution OCT from a multi-MHz swept source," In High-Speed Biomedical Imaging and Spectroscopy VIII, Vol. 12390, pp. 43-46, 2023.

[11] A.F. Fercher, C.K. Hitzenberger, G. Kamp, S.Y. Elzaiat, "Measurement of intraocular distances by backscattering spectral interferometry," Opt. Commun., vol. 117, pp. 43–48, 1995.

[12] E. Brinkmeyer and R. Ulrich, "High-resolution OCDR in dispersive wave-guides," Electronics Letters, vol.6, pp. 413–414, 1990.

[13] S.R. Chinn, E.A. Swanson, and J.G. Fujimoto, "Optical coherence tomography using a frequency-tunable optical source," Opt. Lett. vol. 22, pp.340–342, 1997.

[14] B. Golubovic, B.E. Bouma, G.J. Tearney, and J.G. Fujimoto, "Optical frequency-domain reflectometry using rapid wavelength tuning of a Cr4+: forsterite laser," Opt. Lett. vol. 22, pp. 1704–1706, 1997.

[15] A. F. Fercher, C. K. Hitzenberger, G. Kamp, and S. Y. El-Zaiat, "Measurement of intraocular distances by backscattering spectral interferometry," Optics communications, vol. 117, pp. 43-48, 1995

[16] F. C. K. H. Lexer, C. K. Hitzenberger, A. F. Fercher, and M. Kulhavy, "Wavelength-tuning interferometry of intraocular distances," Applied optics, vol.36, pp.6548-6553, 1997.

[17] G. Hausler, and M. W. Lindner, ""Coherence radar" and "spectral radar" -new tools for dermatological diagnosis," Journal of biomedical optics, vol. 3, pp.21-31, 1998.

[18] M. Wojtkowski, R. Leitgeb, A. Kowalczyk, T. Bajraszewski, and A. F. Fercher, "In vivo human retinal imaging by Fourier domain optical coherence tomography," Journal of biomedical optics, vol.7, pp. 457-463. 2002.

[19] A. P. Ivanov, A. P. Chaikovskii, and A. A. Kumeisha, "New method for high-range resolution measurements of light scattering in optically dense inhomogeneous media," Optics Letters, vol. 1, pp.226-228, 1977.

[20] C. K. Hitzenberger. Low-coherence interferometry from: *Handbook of Visual Optics* CRC Press, 2017.

[21] J. M. Schmitt and G. Kumar, "Optical scattering properties of soft tissue: a discrete particle model," Applied optics, vol.37, pp. 2788-2797, 1998.

[22] R. K. Wang, "Modelling optical properties of soft tissue by fractal distribution of scatterers," Journal of Modern Optics, vol.47, pp. 103-120, 2000.

[23] R. K. Wang and Z. Ma, "Real-time flow imaging by removing texture pattern artifacts in spectral-domain optical Doppler tomography," Optics letters, vol.31, pp. 3001-3003, 2006.

[24] R. Leitgeb, C.K. Hitzenberger, and A.F. Fercher, "Performance of fourier domain vs. time domainoptical coherence tomography," Opt. Express, vol.11, pp.889–894, 2003.

[25] J. F. de Boer, B. Cense, B. H. Park, M. C. Pierce, G. J. Tearney, and B. E. Bouma, "Improved signal-to-noise ratio in spectral-domain compared with time-domain optical coherence tomography," Opt. Lett. vol. 28, pp. 2067–2069, 2003.

[26] M. A. Choma, M. V. Sarunic, C. H. Yang, and J. A. Izatt, "Sensitivity advantage of swept source and Fourier domain optical coherence tomography," Opt. Express, vol. 11, pp. 2183–2189, 2003.

[27] W. Drexler and J. G. Fujimoto, Eds. *Optical coherence tomography: technology and applications*. 2nd ed. Switzerland: Springer International Publishing, Ch. 7, 2015.

[28] A. F. Fercher, W. Drexler, C. K. Hitzenberger, and T. Lasser, "Optical coherence tomography - principles and applications," Reports on progress in physics, vol.66, pp. 239–303, 2003.

[29] W. Drexler and J. G. Fujimoto, Eds. *Optical coherence tomography: technology and applications*. 2nd ed. Switzerland: Springer International Publishing, Ch. 9, 2015.

[30] S. Aumann, S. Donner, J. Fischer, and F. Müller, "Optical coherence tomography (OCT): principle and technical realization," *High resolution imaging in microscopy and ophthalmology: new frontiers in biomedical optics*, pp.59-85, 2019.

[31] U. T. Schwarz, F. Kopp, T. Weig, C. Eichler, and U.Strauss, "Superluminescent light emitting diodes of 100mW output power for pico-projection," Conference on Lasers and Electro-Optics Pacific Rim (CLEO-PR), Optical Society of America, MH2-3, 2013.

[32] N. M. Milani, A. Asgari, "The effects of carrier transport phenomena on the spectral and power characteristics of blue superluminescent light emitting diodes," Physica E, vol.69, pp. 165-170,2015.

[33] L. N. Kurbatov, S. S. Shakhidzhanv, L. V. V. krapukhin, and S. I. Kolonenkova, "Investigation of superluminescence emitted by a gallium arsenide diode," Sov. Phys. Semicond. vol.4, pp. 1739, 1971.

[34] C.C. Culter, S.A. Newton, H.J. Show, "Limitation of rotation sensing by scattering," Opt. Lett. vol. 5, pp. 488–490, 1980.

[35] W. Drexler and J. G. Fujimoto, Eds. *Optical coherence tomography: technology and applications*. 2nd ed. Switzerland: Springer International Publishing, 2015.

[36] N. M. Milani, V. Mohadesi, A. Asgari, "The effects of temperature dependent recombination rates on performance of InGaN/GaN blue superluminescent light emitting diodes," Physica E, vol.71, pp.64-69, 2015.

[37] N. M. Milani, V. Mohadesi, and A. Asgari, "A novel theoretical model for broadband blue InGaN/GaN superluminescent light emitting diodes," Journal of Applied Physics, vol.117, pp.054502, 2015.

[38] N. Matuschek and M. Duelk, "Modeling and simulation of superluminescent light-emitting diodes (SLEDs)," IEEE J. Sel. Top. Quantum Electron. vol. 19, pp. 7800307, 2013.

[39] www.thorlabs.com

[40] S. R. Chinn, E. A. Swanson, J. G. Fujimoto, "Optical coherence tomography using a frequency tunable optical source," Opt. Lett. vol.22, pp. 340–342 1997.

[41] M. A. Choma, M. V. Sarunic, C. H. Yang, and J. A. Izatt, "Sensitivity advantage of swept source and Fourier domain optical coherence tomography," Opt. Express, vol.11, pp. 2183–2189, 2003.

[42] S. H. Yun, G. J. Tearney, J. F. de Boer, N. Iftimia, and B. E. Bouma, "High-speed optical frequency-domain imaging," Opt. Express, vol.11, pp. 2953–2963, 2003.

[43] T. Klein and R. Huber, "High-speed OCT light sources and systems," Biomedical optics express, vol. 8, pp. 828-859, 2017.

[44] S. Chen, B. Potsaid, Y. Li, J. Lin, Y. Hwang, E. M. Moult, J. Zhang, D. Huang, and J. G. Fujimoto, "High speed, long range, deep penetration swept source OCT for structural and angiographic imaging of the anterior eye," Scientific Reports, vol.12, pp. 992 (1-14), 2022.

[45] S. Zheng, Y. Bai, Z. Xu, P. Liu, and G. Ni, "Optical coherence tomography for three-dimensional imaging in the biomedical field: a review," Frontiers in Physics, pp. 552 (1-13), 2021.

[46] W. Drexler and J. G. Fujimoto, Eds. *Optical coherence tomography: technology and applications*. 2nd ed. Switzerland: Springer International Publishing, Ch. 46, 2015.

[47] W. Drexler and J. G. Fujimoto, Eds. *Optical coherence tomography: technology and applications*. 2nd ed. Switzerland: Springer International Publishing, Ch. 41, 2015.

[48] Z. Chen, *Functional optical coherence tomogoraphy, in Frontiers in Biomedical Engineering*, Ed. by N. H. C. Hwang, S. L. -Y. Woo Kluwer Academic/Plenum, New York, 2003.

[49] Z. Chen, T. E. Milner, D. Dave, and J. S. Nelson, "Optical Doppler tomographic imaging of fluid flow velocity in highly scattering media," Opt. Lett. vol. 22, pp. 64–66, 1997.

[50] V. J. Srinivasan, S. Sakadzic, I. Gorczynska, S. Ruvinskaya, W. Wu, J. G. Fujimoto, and D. A. Boas, "Quantitative cerebral blood flow with optical coherence tomography," Opt. Express, vol.18, pp. 2477–2494, 2010

[51] R. A. Leitgeb, L. Schmetterer, W. Drexler, A. F. Fercher, R. J. Zawadzki, and T. Bajraszewski, "Real-time assessment of retinal blood flow with ultrafast acquisition by color Doppler Fourier domain optical coherence tomography," Optics Express, vol. 11, pp. 3116-3121, 2003.

[52] B. R. White, M. C. Pierce, N. Nassif, B. Cense, B. H. Park, G. J. Tearney, B. E. Bouma, T. C. Chen, and J. F. de Boer, "In vivo dynamic human retinal blood flow imaging using ultra-high-speed spectral domain optical Doppler tomography," Optics express, vol. 11, pp.3490-3497, 2003.

[53] S. Yazdanfar, A. M. Rollins, and J. A. Izatt, "Imaging and velocimetry of the human retinal circulation with color Doppler optical coherence tomography," Optics letters, vol. 25, pp. 1448-1450, 2000.

[54] R. A. Leitgeb, L. Schmetterer, C. K. Hitzenberger, A. F. Fercher, F. Berisha, M. Wojtkowski, and T. Bajraszewski, "Real-time measurement of in vitro flow by Fourier-domain color Doppler optical coherence tomography," Optics letters, vol. 29, 171-173, 2004.

[55] J. Ong, A. Zarnegar, G. Corradetti, S. R. Singh, and J. Chhablani, "Advances in optical coherence tomography imaging technology and techniques for choroidal and retinal disorders," Journal of Clinical Medicine, vol. 11, pp. 5139, 2022.

[56] B. H. Park, C. Saxer, S. M. Srinivas, J. S. Nelson, and J. F. de Boer, "In vivo burn depth determination by high-speed fiber-based polarization sensitive optical coherence tomography," J. Biomed. Opt. vol. 6, pp. 474–479, 2001.

[57] B. Cense, T. C. Chen, B. H. Park, M. C. Pierce, and J. F. de Boer, "In vivo depth-resolved birefringence measurements of the human retinal nerve fiber layer by polarization-sensitive optical coherence tomography," Opt. Lett. vol. 27, pp. 1610–1612, 2002.

[58] B. Cense, T. C. Chen, B. H. Park, M. C. Pierce, and J. F. de Boer, "Thickness and birefringence of healthy retinal nerve fiber layer tissue measured with polarization-sensitive optical coherence tomography," Invest. Ophthalmol. Vis. Sci. vol. 45, pp. 2606–2612, 2004.

[59] D. Fried, J. Xie, S. Shafi, J. D. B. Featherstone, T. M. Breunig, and C. Le, "Imaging caries lesions and lesion progression with polarization sensitive optical coherence tomography," J. Biomed. Opt. vol. 7, pp. 618–627, 2002.

[60] E. Götzinger, M. Pircher, B. Baumann, C. Ahlers, W. Geitzenauer, U. Schmidt-Erfurth, and C. K. Hitzenberger, "Three-dimensional polarization sensitive OCT imaging and interactive display of the human retina," Optics express, vol. 17, pp.4151-4165, 2009.

[61] M. Yamanari, S. Makita, Y. Lim, and Y. Yasuno, "Full-range polarization-sensitive swept-source optical coherence tomography by simultaneous transversal and spectral modulation," Opt Express, vol.18, pp.13964–13980, 2010.

[62] R. G. Sayegh, S. Zotter, P. K. Roberts, M. M. Kandula, S. Sacu, D. P. Kreil, B. Baumann, M. Pircher, C. K. Hitzenberger, and U. Schmidt-Erfurth, "Polarization-Sensitive Optical Coherence Tomography and Conventional Retinal Imaging Strategies in Assessing Foveal Integrity in Geographic Atrophy," Investig. Ophthalmol. Vis. Sci, vol. 56, pp. 5246–5255, 2015.

[63] M. Pircher, C. K. Hitzenberger, U. Schmidt-Erfurth, "Polarization sensitive optical coherence tomography in the human eye," Prog. Retin. Eye Res. vol. 30, pp. 431–451, 2011.

[64] Y. Ueno, H. Mori, K. Kikuchi, M. Yamanari, and T. Oshika, "Visualization of Anterior Chamber Angle Structures With Scattering- and Polarization-Sensitive Anterior Segment Optical Coherence Tomography," Transl. Vis. Sci. Technol. vol.10, pp. 1-9 2021,

[65] W. Drexler, "Ultrahigh-resolution optical coherence tomography," J. Biomed. Opt. vol. 9, pp. 47–74, 2004.

[66] R. F. Spaide and D. R. Lally, "High Resolution Spectral Domain Optical Coherence Tomography of Multiple Evanescent White Dot Syndrome," Retinal Cases and Brief Reports, 2022.

[67] W. Drexler and J. G. Fujimoto, Eds. *Optical coherence tomography: technology and applications*. 2nd ed, Switzerland: Springer International Publishing, Ch. 25, 2015.

[68] L. Vabre, A. Dubois, and A. C. Boccara, "Thermal-light full-field optical coherence tomography," Opt. Lett. vol. 27, pp. 530–532, 2002.

[69] A. Dubois, L. Vabre, A. C. Boccara, and E. Beaurepaire, "High-resolution full-field optical coherence tomography with a Linnik microscope," Appl. Opt. vol. 41, pp. 805–812, 2002.

[70] A. Dubois, K. Grieve, G. Moneron, R. Lecaque, L. Vabre, and A. C. Boccara, "Ultrahigh-resolution full-field optical coherence tomography," Appl. Opt. vol. 43, pp.2874–2882, 2004.

[71] A. Dubois, G. Moneron, K. Grieve, and A. C. Boccara, "Three-dimensional cellular-level imaging using full-field optical coherence tomography," Phys. Med. Biol. vol. 49, pp. 1227–1234, 2004.

[72] E. Beaurepaire, A. C. Boccara, M. Lebec, L. Blanchot, and H. Saint-Jalmes, "Full-field optical coherence microscopy," Opt. Lett. vol. 23, pp. 244–246, 1998.

[73] K. Grieve, O. Thouvenin, A. Sengupta, V. M. Borderie, and M. Paques, "Appearance of the Retina With Full-Field Optical Coherence Tomography," Investig. Ophthalmol. Vis. Sci. vol. 57, OCT96–OCT104, 2016.

[74] S. Song, J. Xu, and R. K. Wang, "Long-range and wide field of view optical coherence tomography for in vivo 3D imaging of large volume object based on akinetic programmable swept source," Biomed. Opt. Express, vol.7, pp.4734–4748, 2016.

[75] T. Klein, W. Wieser, C. M. Eigenwillig, B. R. Biedermann, and R. Huber, "Megahertz OCT for ultrawide-field retinal imaging with a 1050 nm Fourier domain mode-locked laser," Opt. Express, vol. 19, pp. 3044–3062, 2011.

[76] R. Huber, M. Wojtkowski, and J. G. Fujimoto, "Fourier domain mode locking (FDML): a new laser operating regime and applications for optical coherence tomography," Opt Express. vol. 14, pp. 3225–3237, 2006.

[77] K. J. Parker, M. M. Doyley, and D. J. Rubens, "Imaging the elastic properties of tissue: the 20 year perspective," Phys. Med. Biol. vol. 56, R1, 2011.

[78] J. M. Schmitt, "OCT elastography: imaging microscopic deformation and strain of tissue," Opt. Express, vol. 3, pp. 199–211, 1998.

[79] J. Ophir, I. Cespedes, H. Ponnekanti, Y. Yazdi, and X. Li, "Elastography: a quantitative method for imaging the elasticity of biological tissues," Ultrason. Imaging, vol. 13, pp. 111–134, 1991.

[80] R. Muthupillai, D. J. Lomas, P. J. Rossman, J. F. Greenleaf, A. Manduca, and R. L. Ehman, "Magnetic resonance elastography by direct visualization of propagating acoustic strain waves," Science, vol. 269, pp. 1854–1857, 1995.

[81] H. W. Babcock, "The possibility of compensating astronomical seeing," In Publications of the Astronomical Society of the Pacific, 386th Ed.; The Astronomical Society of the Pacific: San Francisco, WI, USA, vol. 65, pp. 229–236, 1953.

[82] B. Povazay, K. Bizheva, A. Unterhuber, B. Hermann, H. Sattmann, A. F. Fercher, W. Drexler, A. Apolonski, W. J. Wadsworth, J. C. Knight, and P. S. J. Russell, "Submicrometer axial resolution optical coherence tomography," Optics letters, vol. 27, pp.1800-1802, 2002.

[83] J. Yi, W. Liu, S. Chen, V. Backman, N. Sheibani, C. M. Sorenson, A. A. Fawzi, R. A. Linsenmeier, and H. F. Zhang, "Visible light optical coherence tomography measures retinal oxygen metabolic response to systemic oxygenation," Light: Science & Applications, vol. 4, pp. e334-e334, 2015.

[84] J. P. Ehlers, D. S. Petkovsek, A. Yuan, R. P. Singh, and S. K. Srivastava, "Intrasurgical assessment of subretinal tPA injection for submacular hemorrhage in the PIONEER study utilizing intraoperative OCT," Ophthalmic Surg. Lasers Imaging Retin. vol. 46, pp. 327–332, 2015.

[85] D. S. Grewal, O. M. Carrasco-Zevallos, R. Gunther, J. A. Izatt, C. A. Toth, and P. Hahn, "Intra-operative microscope-integrated swept-source optical coherence tomography guided placement of Argus II retinal prosthesis," Acta Ophthalmol. vol.95, pp. e431–e432, 2017.

[86] S. A. Boppart, B. E. Bouma, C. Pitris, G. J. Tearney, J. F. Southern, M. E. Brezinski, and J. G. Fujimoto, "Intraoperative assessment of microsurgery with three-dimensional optical coherence tomography," Radiology, vol. 208, pp. 81–86, 1998.

[87] S. A. Boppart, M. E. Brezinski, C. Pitris, and J. G. Fujimoto, "Optical coherence tomography for neurosurgical imaging of human intracortical melanoma," Neurosurgery, vol. 43, pp. 834–841, 1998.

[88] G. Song, K. K. Chu, S. Kim, M. Crose, B. Cox, E. T. Jelly, J. N. Ulrich, and A. Wax, "First Clinical Application of Low-Cost OCT. Transl," Vis. Sci. Technol. vol.8, p.61, 2019.

[89] S. R. Rufai, "Handheld optical coherence tomography removes barriers to imaging the eyes of young children," Eye, vol. 36, pp. 907–908, 2022.

[90] R. Nicholson, D. Osborne, L. Fairhead, L. Beed, C. M. Hill, and H. Lee, "Segmentation of the foveal and parafoveal retinal architecture using handheld spectral-domain optical coherence tomography in children with Down syndrome," Eye, vol. 36, pp. 963–968, 2022.

[91] R. S. Maldonado, J. A. Izatt, N. Sarin, D. K. Wallace, S. Freedman, C. M. Cotten, and C. A. Toth, "Optimizing hand-held spectral domain optical coherence tomography imaging for neonates, infants, and children," Investig. Ophthalmol. Vis. Sci., vol. 51, pp. 2678–2685, 2010.

[92] S. Radhakrishnan, A. M. Rollins, J. E. Roth, S. Yazdanfar, V. Westphal, D. S. Bardenstein, J. A. Izatt, "Real-time optical coherence tomography of the anterior segment at 1310 nm," Arch. Ophthalmol. vol. 119, pp. 1179 (1-7), 2001.

[93] X. Li, C. Chudoba, T. Ko, C. Pitris, and J. G. Fujimoto, "Imaging needle for optical coherence tomography," Opt. Lett. vol. 25, pp. 1520–1522, 2000.

[94] R. A. McLaughlin, B. C. Quirk, A. Curatolo, R. W. Kirk, L. Scolaro, D. Lorenser, P. D. Robbins, B. A. Wood, C. M. Saunders, and D. D. Sampson, "Imaging of breast cancer with optical coherence tomography needle probes: feasibility and initial results," IEEE J. Sel. Top. Quantum Electron. vol. 18, pp. 1184–1191, 2012.

[95] N. V. Iftimia, B. E. Bouma, M. B. Pitman, B. Goldberg, J. Bressner, and G. J. Tearney, "A portable, low coherence interferometry based instrument for fine needle aspiration biopsy guidance," Rev. Sci. Instrum. vol. 76, pp. 064301–064306 (1-7), 2005.

[96] R. A. McLaughlin, X. Yang, B. C. Quirk, D. Lorenser, R. W. Kirk, P. B. Noble, and D. D. Sampson, "Static and dynamic imaging of alveoli using optical coherence tomography needle probes," J. Appl. Physiol. vol. 113, pp. 967–974, 2012.

[97] K. Tan, M. Shishkov, A. Chee, M. Applegate, B. Bouma, and M. Suter, "Flexible

transbronchial optical frequency domain imaging smart needle for biopsy guidance," Biomed. Opt. Express, vol. 3, pp. 1947–1954, 2012.

[98] S. Han, M. V. Sarunic, J. Wu, M. Humayun, and C. Yang, "Handheld forward-imaging needle endoscope for ophthalmic optical coherence tomography inspection," J. Biomed. Opt. vol. 13, p. 020505 (1-3), 2008.

[99] M. Zhao, Y. Huang, and J. U. Kang, "Sapphire ball lens-based fiber probe for common-path optical coherence tomography and its applications in corneal and retinal imaging," Opt. Lett. vol. 37, pp. 4835–4837, 2012.

[100] M. S. Jafri, S. Farhang, R. S. Tang, N. Desai, P. S. Fishman, R. G. Rohwer, C. M. Tang, and J. M. "Schmitt, Optical coherence tomography in the diagnosis and treatment of neurological disorders," J. Biomed. Opt. vol. 10, pp. 051603 (1-11), 2005.

[101] C. Sun, K. K. Lee, B. Vuong, M. D. Cusimano, A. Brukson, A. Mauro, N. Munce, B. K. Courtney, B. A. Standish, and V. X. Yang, "Intraoperative handheld optical coherence tomography forward-viewing probe: physical performance and preliminary animal imaging," Biomed. Opt. Express, vol. 3, pp. 1404 (1-9), 2012.